Optical and vibrational properties of MnF_6^{4-} complexes in cubic fluoroperovskites: insight through embedding calculations using Kohn–Sham equations with constrained electron density

2006 J. Phys.: Condens. Matter 18 1519

(http://iopscience.iop.org/0953-8984/18/5/004)

INSTITUTE OF PHYSICS PUBLISHING JOURNAL OF PHYSICS: CONDENSED MATTER

J. Phys.: Condens. Matter **18** (2006) 1519–1534 doi:10.1088/0953-8984/18/5/004

Optical and vibrational properties of MnF_6^{4-} complexes in cubic fluoroperovskites: insight through embedding calculations using Kohn–Sham equations with constrained electron density

J M García-Lastra[1], T Wesolowski[2], M T Barriuso[1], J A Aramburu[3] and M Moreno[3]

[1] Departamento de Física Moderna, Universidad de Cantabria, Avenida de los Castros s/n, 39005 Santander, Spain
[2] Depártement de Chimie, Université de Genève, 30, quai Ernest-Ansermet, CH-1211 Genève 4, Switzerland
[3] Departamento de Ciencias de la Tierra y Física de la Materia Condensada, Universidad de Cantabria, Avenida de los Castros s/n, 39005 Santander, Spain

Received 5 September 2005
Published 17 January 2006
Online at stacks.iop.org/JPhysCM/18/1519

Abstract

The local structure and optical and vibrational properties associated with Mn^{2+}-doped cubic AMF_3 (A = K, Rb; M = Mg, Zn, Cd) fluoroperovskites are studied by means of embedding calculations using Kohn–Sham equations with constrained electron density. It is shown that while an electronic parameter like $10Dq$ essentially depends on the Mn^{2+}–F^- distance, the local vibration frequencies ω_i ($i = a_{1g}$, e_g modes) are dominated by the interaction between F^- ligands and nearest M^{2+} ions lying along bonding directions. The high ω_a values observed for $KMgF_3$:Mn^{2+} and $KZnF_3$:Mn^{2+}, the huge variations of ω_e and ω_a frequencies when the host lattice is changed, as well as the increase of Huang–Rhys factors and the Stokes shift following the host lattice parameter, are shown to be related to this elastic coupling of the MnF_6^{4-} complex to the rest of the host lattice. The present results support the conclusion that the Stokes shift is determined by the interaction of the excited $^4T_{1g}$ state with a_{1g} and e_g local modes while the coupling with the t_{2g} shear mode is not relevant. The variations of local vibrational frequencies and the Stokes shift induced by a hydrostatic pressure on a given system are shown to be rather different to those produced by the chemical pressure associated with distinct host lattices.

1. Introduction

The presence of a substitutional transition metal impurity, M, in an insulating or semiconducting lattice gives rise to new physico-chemical properties. In the case of insulating

host lattices active electrons are usually localized in the ML_N complex formed by the impurity and the N nearest neighbours or ligands which are lying at a distance R from the metal [1–3]. The properties associated with an impurity thus depend on the actual equilibrium geometry in the ground and first excited states of the ML_N complex, which in turn reflects its interaction with close ions of the rest of the lattice. This argument stresses the importance of describing properly the embedding of a complex within the whole lattice for a proper understanding of its associated properties.

The present work is aimed at exploring the local structure and optical and vibrational properties associated with Mn^{2+} impurities in cubic AMF_3 fluoroperovskites [4–14] by means of a recent method for improving the embedding in the realm of the density functional theory (DFT) [15–17]. In this method the electronic density of a finite cluster is divided into two regions. In the first region, the electronic density of active electrons, which will be denoted here as $\rho_{\rm I}(\mathbf{r})$, is constructed using a set of embedded orbitals, $\phi_{\rm I}^i$. The density $\rho_{\rm II}(\mathbf{r})$ corresponding to the other part of the cluster is frozen and it is used to express the effective potential in the Kohn–Sham-like one-electron equations for the orbitals $\phi_{\rm I}^i$. These equations will be denoted as Kohn–Sham equations with constrained electron density (KSCED) throughout this work. Since the KSCED effective potential is expressed by means of the bi-functional of non-additive kinetic energy of unknown analytic form, not all embedded systems can be treated by means of the KSCED embedding formalism. In particular, the recently developed gradient-dependent approximation [15] is adequate only for such systems for which the overlap between $\rho_{\rm I}(\mathbf{r})$ and $\rho_{\rm II}(\mathbf{r})$ is small. Among the possible systems falling into this category are such materials in which the active electrons are well localized [16].

In the present study on Mn^{2+} impurities in cubic fluoroperovskites particular attention is addressed to exploring the Stokes shift, a quantity which has a great influence not only for determining the relaxation in an excited state (placed at energy $E_{\rm exc}$ above the ground state) but especially for its implications on the radiative emission probability. In fact, it has been stressed [18–20, 13] that an increase of the Stokes shift *keeping* $E_{\rm exc}$ favours the luminescence quenching. A good insight into this problem thus requires one first to explore the Stokes shift in model systems where high symmetry is of great help for clarifying its microscopic origin.

In the case of doped insulating materials the Stokes shift arises basically from the linear coupling of the electronic excited state responsible for the emission with local vibrational modes [21–28]. Due to the localized character of active electrons in both ground and excited states such modes involve basically the distortion of ligands. Experimental evidence on these modes can sometimes be obtained from low-temperature emission or absorption spectra [28, 8]. In the non-radiative decay process it has been shown that energy is transferred in a first step to local modes and later to lattice modes [29].

In MnF_6^{4-} complexes in cubic fluoroperovskites luminescence arises *only* from the first $^4T_{1g}$ crystal field state which depends on the cubic field splitting parameter $10Dq$ [7, 8, 10, 30]. For a T_{1g} excited state a linear Jahn–Teller coupling with e_g and t_{2g} modes is symmetry allowed together with the coupling to the full symmetric a_{1g} mode [13, 21, 24]. The Stokes shift thus depends on the $\omega_{\rm e}$, $\omega_{\rm t}$ and $\omega_{\rm a}$ frequencies of e_g, t_{2g} and a_{1g} modes, respectively, in the ground state and also on the corresponding constants (termed $V_{\rm e}$, $V_{\rm t}$ and $V_{\rm a}$, respectively) describing the coupling with the first excited state $^4T_{1g}$.

Mn^{2+}-doped cubic fluoroperovskites are *model systems* whose equilibrium impurity–ligand distance, R_0, has been explored by different methods [5–7, 12]. However, there are several important questions which need to be clarified:

(1) In the interpretation of electronic parameters like $10Dq$ or the superhyperfine tensor it has been assumed that they depend only on R_0 but not on the nature of the host lattice

where the complex is embedded [6, 7]. Although this important simplification seems to be reasonably consistent with available experimental findings no detailed theoretical study has been carried out up to now for exploring its validity.

(2) At variance with results for electronic parameters it has recently been pointed out [13] that frequencies of local modes are however sensitive not only to the equilibrium impurity–ligand distance at $P = 0$ atm, R_0, but *also* to the nature of the host lattice where the complex is placed. This relevant difference between electronic and vibrational properties thus deserves a further investigation.

(3) The Stokes shift of Mn^{2+} complexes in cubic fluoroperovskites has been explained up to now considering the coupling of the $^4T_{1g}$ excited state *only* with stretching e_g and a_{1g} local modes, thus ignoring the t_{2g} bending mode [13, 26].

(4) Luminescence spectra of $KMgF_3$:Mn^{2+} at $T = 5$ K [8] reveal a weak progression involving a mode whose frequency is 570 cm^{-1} and a Huang–Rhys factor certainly smaller than the unity. Recent DFT calculations on clusters of 21 atoms with a point charges embedding suggest [12] that such a frequency can reasonably be associated with the local a_{1g} mode. However, this assignment is surprising as $\hbar\omega_a = 538$ cm^{-1} for FeF_6^{3-} [31] and usually trivalent ions lead to higher vibrational frequencies when compared to divalent ions if both ligand ion and coordination number are the same [32].

(5) The variation experienced by the Stokes shift when a cubic fluoroperovskite is replaced by another one has been suggested [13] to be different to that induced by a hydrostatic pressure on a given system keeping the same the variation of the metal–ligand distance, R. This statement certainly requires a further investigation.

The present work is aimed at investigating all these questions using the KSCED embedding formalism. For the sake of completeness some standard Kohn–Sham (KS) calculations for the whole cluster and using a point charges embedding are also reported. The present work is divided as follows. Section 2 is devoted to provide with details about the KSCED orbital-free embedding formalism used in the calculations. In section 3 a brief outline on the linear coupling between a T state and local modes and its influence on the Stokes shift is included. Section 4 collects the main results obtained in this work as well as an analysis of them, while in the last section some final considerations are reported.

2. Theoretical: the KSCED orbital-free embedding formalism

The ground-state electron density of an embedded molecule in a given environment can be derived from one-electron equations [33]:

$$\{-\nabla^2/2 + V_{\text{eff}}^{\text{KSCED}}[\rho_{\text{I}}, \rho_{\text{II}}](\mathbf{r})\}\phi_i^{\text{KSCED}}(\mathbf{r}) = \varepsilon_i^{\text{KSCED}}\phi_i^{\text{KSCED}}(\mathbf{r}) \tag{1}$$

where $\rho_{\text{I}} = 2\sum_{i=1}^{N} \phi_i^{\text{KSCED}*}(\vec{r})\phi_i^{\text{KSCED}}(\vec{r})$ is the electron density of the embedded system constructed using one-electron functions and ρ_{II} is the electron density of the environment. Atomic units are applied in all equations throughout the text. The superscript KSCED is used to indicate that such quantities as the effective potential, orbitals, and orbital energies, differ from the corresponding quantities occurring in Kohn–Sham [34] equations:

$$\{-\nabla^2/2 + V_{\text{eff}}^{\text{KS}}[\rho](\mathbf{r})\}\phi_i^{\text{KS}}(\mathbf{r}) = \varepsilon_i^{\text{KS}}\phi_i^{\text{KS}}(\mathbf{r}) \tag{2}$$

where $\rho = 2\sum_{i=1}^{N} \phi_i^{\text{KS}*}(\vec{r})\phi_i^{\text{KS}}(\vec{r})$.

The effective potential in equation (1) differs from that in equation (2) by additional terms describing the interactions between the two subsystems. These terms have a universal system-

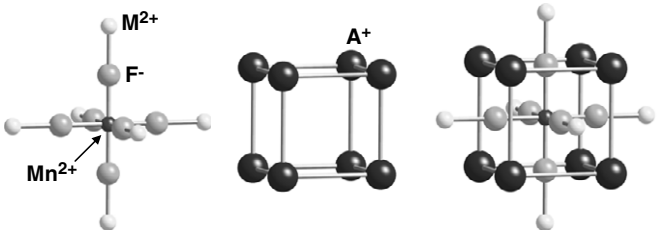

Figure 1. 13 + 8 cluster used in the KSCED calculations. There are 13 ions in the region I, while region II (where the electronic density is frozen) involves 8 ions.

independent form [33] reading

$$V_{\mathrm{eff}}^{\mathrm{emb(KSCED)}}[\rho_{\mathrm{I}}, \rho_{\mathrm{II}}](\mathbf{r}) = -\sum_{\alpha} Z_{\alpha}^{\mathrm{II}}/|\mathbf{R}_{\alpha}^{\mathrm{II}} - \mathbf{r}| + \int \rho_{\mathrm{II}}(\mathbf{r}')\,\mathrm{d}\mathbf{r}'/|\mathbf{r} - \mathbf{r}'| + \delta E_{\mathrm{xc}}[\rho]/\delta\rho|_{\rho=\rho\mathrm{I}+\rho\mathrm{II}} - \delta E_{\mathrm{xc}}[\rho]/\delta\rho|_{\rho=\rho\mathrm{I}} + \delta T_{\mathrm{s}}^{\mathrm{nad}}[\rho_{\mathrm{I}}, \rho_{\mathrm{II}}]/\delta\rho|_{\rho=\rho\mathrm{I}} \tag{3}$$

where N_{II} is the number of nuclei in subsystem II and Z_{α}^{II} is the nuclear charge of nucleus α in subsystem II. The exchange–correlation functional $E_{\mathrm{xc}}[\rho]$ is defined as in the KS formalism [34] and the non-additive kinetic energy $T_{\mathrm{s}}^{\mathrm{nad}}[\rho_{\mathrm{I}}, \rho_{\mathrm{II}}]$, a functional depending on two-electron densities, is defined as

$$T_{\mathrm{s}}^{\mathrm{nad}}[\rho_{\mathrm{I}}, \rho_{\mathrm{II}}] = T_{\mathrm{s}}[\rho_{\mathrm{I}} + \rho_{\mathrm{II}}] - T_{\mathrm{s}}[\rho_{\mathrm{I}}] - T_{\mathrm{s}}[\rho_{\mathrm{II}}] \tag{4}$$

where $T_{\mathrm{s}}[\rho]$ is the kinetic energy of the reference system of the non-interacting electrons.

Equations (1) and (2) have different solutions, which depend on the environment represented in the KSCED embedding potential by means of positions and electric charges of atomic nuclei and the electron density of the environment. KSCED calculations have been performed by means of a modified deMon code [35]. The following approximations are used in these equations: (i) the Becke–Perdew approximation [36, 37] is used for $E_{\mathrm{xc}}[\rho]$ and (ii) the non-additive kinetic energy functional is of the generalized gradient approximation (GGA) form proposed in [15], in which the gradient-dependency of $T_{\mathrm{s}}[\rho]$ takes the form proposed by Lembarki and Chermette [38]. Such an approximation $T_{\mathrm{s}}^{\mathrm{nad}}[\rho_{\mathrm{I}},\rho_{\mathrm{II}}]$ was demonstrated to be adequate for the cases where the ρ_{I}, ρ_{II} overlap is small. The basis sets of the DZVP quality (double-ζ GTO plus five polarization functions) was used in all embedding calculations.

In the KSCED embedding calculations, two different models of the environment have been used. In the first one (called 13 + 8, figure 1), there are 13 ions in the region I, while region II (where the electronic density is frozen) involves 8 ions. Therefore, there are 6 ions outside the MnF_6^{4-} complex lying also in the region I. In the second model (called 21 + 36, figure 2), there are 21 and 36 ions in regions I and II, respectively. The electrostatic effect of the rest of lattice has been simulated in both cases by means of point charges surrounding the clusters.

Conventional DFT calculations in the KS framework have been performed using the 2004 version of the Amsterdam Density Functional (ADF) code [39]. In these calculations a unique cluster of 21 atoms (similar to the 13 + 8 cluster of the KSCED calculations) has been used. In order to compare with the KSCED results, the same GGA functional and electrostatic potential have been employed. TZP quality basis sets (triple-ζ STO plus one polarization function) have been employed in these calculations. The core electrons (1s–3p for Mn and 1s for F) were kept frozen.

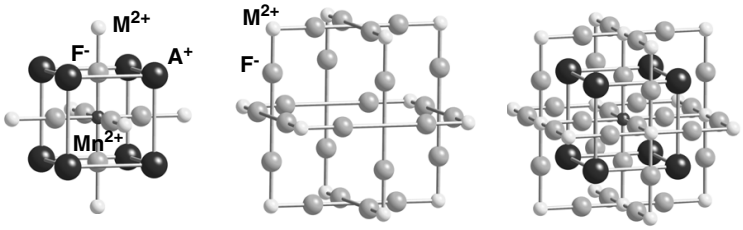

Figure 2. 21 + 36 cluster. There are 21 and 36 ions in regions I and II, respectively.

3. Coupling of $^4T_{1g}$ excited state with local modes: Stokes shift

When luminescence from Mn^{2+} impurities in cubic fluoride lattices is observed it comes only from the $^4T_{1g} \rightarrow {}^6A_{1g}$ transition involving the first excited state $^4T_{1g}$. Other possible luminescence channels are normally quenched [8, 10, 30]. For Mn^{2+}-doped fluorides the first excited state $^4T_{1g}$ lies well below the bottom of the conduction band of the host lattice [40] and thus there is not the anomalous luminescence observed for divalent rare earth cations like Tm^{2+}, Yb^{2+} or Eu^{2+} [41, 42]. The existence of Stokes shift reflects an equilibrium geometry in the first excited state different to that of the ground state. This fact in turn underlines the *localized character* of active electrons involved in the MnF_6^{4-} complex. The changes of equilibrium geometry in MnF_6^{4-} on passing from $^6A_{1g}$ to $^4T_{1g}$ are usually described through the linear coupling with local modes [43, 21, 13]. For an octahedral complex a T state can be coupled linearly only to e_g and t_{2g} modes, in addition to the symmetric a_{1g} mode which is always allowed. Working in the $\{xz, yz, xy\}$ basis of the triplet T state, this coupling is pictured by the following effective Hamiltonian:

$$H_{\text{eff}} = V_a \mathbf{I} Q_a + V_e(\mathbf{U}_\theta Q_\theta + \mathbf{U}_\varepsilon Q_\varepsilon) + V_t(\mathbf{U}_{xy} Q_{xy} + \mathbf{U}_{xz} Q_{xz} + \mathbf{U}_{yz} Q_{yz}). \tag{5}$$

Here $\mathbf{I}$ means the identity 3×3 matrix while $\mathbf{U}_\theta$, $\mathbf{U}_\varepsilon$ and $\mathbf{U}_{xy}$ matrices [21] are given by

$$\mathbf{U}_\theta = \begin{pmatrix} \frac{1}{2} & 0 & 0 \\ 0 & \frac{1}{2} & 0 \\ 0 & 0 & -1 \end{pmatrix}; \qquad \mathbf{U}_\varepsilon = \begin{pmatrix} \frac{-\sqrt{3}}{2} & 0 & 0 \\ 0 & \frac{\sqrt{3}}{2} & 0 \\ 0 & 0 & 0 \end{pmatrix}; \qquad \mathbf{U}_{xy} = \begin{pmatrix} 0 & -1 & 0 \\ -1 & 0 & 0 \\ 0 & 0 & 0 \end{pmatrix}. \tag{6}$$

The coupling with these modes induces a decrease of the energy minimum corresponding to the $^4T_{1g}$ state. The energy decrement induced by the i mode, E_i ($i = a_{1g}$, e_g and t_{2g}), is just given by [21, 13]

$$E_i = V_i^2/2M_L\omega_i^2 = S_i\hbar\omega_i \qquad i = a_{1g},\ e_g \tag{7}$$

$$E_t = (2/3)(V_t^2/2M_L\omega_t^2) \tag{8}$$

where M_L stands for the ligand mass, and S_a and S_e denote the Huang–Rhys factors related to a_{1g} and e_g modes, respectively.

In the case of Cr^{3+}, V^{2+} or Mn^{2+} octahedral complexes there is not experimental evidence of a significant coupling with the shear t_{2g} mode [28, 44–46, 8]. By contrast, low-temperature luminescence spectra sometimes reveal [22, 28, 44–46] the existence of vibrational progressions involving both a_{1g} and e_g stretching modes. Additional light on this matter will be provided in section 4 by comparing the calculated values of V_a, V_e and V_t constants.

It is worth noting that if only the a_{1g} and e_g local modes are important the coupling with the non-symmetric Jahn–Teller mode does not modify the shape of an optical transition from a singlet to a triplet state [47]. Nevertheless, it produces additional vibrational progressions to those coming from the a_{1g} mode [44–46]. In this situation the Stokes shift can simply be written as [44, 10, 13]

$$E_S = E_S^0 + 2\hbar\omega_u \tanh(\hbar\omega_u/2k_BT) \tag{9}$$

$$E_S^0 = 2(S_a\hbar\omega_a + S_e\hbar\omega_e). \tag{10}$$

The second term in (9) simply reflects that d–d transitions for an octahedral complex are parity forbidden and thus progressions at $T = 0$ K start not at zero phonon lines but at the so-called false origins separated from it by the $\hbar\omega_u$ energy corresponding to the odd vibrational mode enabling the transition [44]. As the experimental E_S values for Mn^{2+}-doped cubic fluoroperovskites lie in the 1200–1600 cm^{-1} region [10] and $\hbar\omega_u \approx 250\ cm^{-1}$, the odd phonon contribution to (9) is certainly small when compared to E_S^0.

When a hydrostatic pressure is applied on a given system the variations of V_a and V_e coupling constants and ω_a and ω_e frequencies around the distance corresponding to equilibrium at $P = 0$ atm are described by [13, 24, 26]

$$V_i = C_i R^{-n_i} \qquad i = a_{1g},\ e_g \tag{11}$$

$$\gamma_i = -\partial L\omega_i/\partial LV = -(1/3)(\partial L\omega_i/\partial LR) \qquad i = a_{1g},\ e_g. \tag{12}$$

Therefore, the exponents n_i and the Grüneisen constants γ_i ($i = a, e$) are behind the sensitivity of Huang–Rhys factors and the Stokes shift to a hydrostatic pressure. It is worth noting that for the first excited state $^4T_{1g}$ of a MnF_6^{4-} complex V_a is practically equal to $-(\partial 10Dq/\partial R)$. This just means that [26]

$$n_a \approx n + 1 \tag{13}$$

where n is the exponent reflecting the sensitivity of $10Dq$ to R variations:

$$10Dq = KR^{-n}. \tag{14}$$

Due to the localized character of active electrons it can be expected that the same change in $10Dq$ is produced either by a hydrostatic pressure or by placing the MnF_6^{4-} complex in another isomorphous host lattice provided the R change, ΔR, is the same. However, this idea is no longer true when local vibrational frequencies are concerned [13]. In fact, as the complex is in general elastically coupled to close ions of the rest of the lattice, local vibration frequencies can be modified by changing the nature of such ions *even* if R is kept. Therefore, the variations of ω_i, $\Delta\omega_i$ ($i = a, e$), due to the replacement of a host lattice by another isomorphous one (change of chemical pressure) are not necessarily equivalent to those induced by a hydrostatic pressure on a given system [13]. A simple way of quantifying such a difference is through the chemical Grüneisen parameter γ_i^c. Let us consider two lattices, L_A and L_B, where the same complex is embedded. If ω_i ($i = a, e$) and R_0 denote the frequencies and equilibrium R values at zero hydrostatic pressure for L_A while the values for L_B are described by $\omega_i + \Delta\omega_i$ and $R_0 + \Delta R$, respectively, then the chemical Grüneisen parameter is defined by

$$\gamma_i^c = -(1/3)(\Delta\omega_i/\Delta R)(R_0/\omega_i) \qquad i = a_{1g},\ e_g. \tag{15}$$

In a similar way $10Dq$ values of different AMF_3:Mn^{2+} systems at zero pressure can also be compared. Assuming that along the fluoroperovskites series it can also be written

$$10Dq = KR^{-n^c} \tag{16}$$

then the $10Dq$ variations due to changes of chemical pressure are described through the n^c exponent. Exponents n_i^c ($i = a, e$) reflecting the sensitivity of V_a and V_e coupling constants under chemical pressure are defined in a similar way to equation (16).

Table 1. Mn^{2+}–F^- equilibrium distances, R_0, obtained in KSCED and KS calculations. Experimental distances [6, 7, 10, 12] are also shown (errors are given in parentheses). Units are in Å.

		Calculated			Experimental	
Lattice	R_H	KSCED (13 + 8)	KSCED (21 + 36)	KS	EPR	Optical
$KMgF_3$	1.986	2.064	2.043	2.067	2.07 (1)	2.068 (4)
$KZnF_3$	2.027	2.107	2.090	2.103	2.084 (6)	2.080 (4)
$RbCdF_3$	2.200	2.166	2.162	2.158	2.124 (6)	2.134 (4)
$RbCaF_3$	2.228	2.130	2.127	2.176	2.142	2.131

4. Results and discussion

4.1. Equilibrium geometry for the ground state

The equilibrium Mn^{2+}–F^- distances, R_0, for several Mn^{2+}-doped fluoroperovskites calculated through different procedures are collected in table 1. In these calculations of R_0 only the Mn^{2+}–F^- distance is left as a variable. This assumption is reasonable [12] provided $(R_0 - R_H)/R_H \ll 1$, where R_H means the M–F distance of the perfect AMF_3 host lattice. This condition is reasonably fulfilled as R_0 differs from R_H by less than 4%. Moreover, in table 1 the results obtained by KSCED and conventional KS calculations are compared with those derived through previous determinations of R_0 from the analysis of experimental $10Dq$ and isotropic superhyperfine constants [6, 7, 10, 12, 13]. Bearing in mind that errors involved in calculated distances through DFT are ∼1%, the comparison between R_0 values derived from experimental data and those reported in this work is reasonable. As R_0 figures from the 13 + 8 and 21 + 36 schemes are quite similar the first scheme with less computational cost will be henceforth employed. Only in a few cases have data through the 21 + 36 procedure also been derived. We have verified that if in region I only the 7 ions of the MnF_6^{4-} complex are included the computed R_0 values differ more from experimental ones as it could be expected.

From a physical standpoint, the results embodied in table 1 show that R_0 values for MnF_6^{4-} complexes do depend on the host lattice, pointing out that the MnF_6^{4-} complex has some elastic coupling with close ions of the rest of the lattice. By comparing the same complex in two similar lattices, some information about this elastic coupling is given by the f parameter, defined by

$$f = \Delta R_0 / \Delta R_H. \tag{17}$$

From table 1 a value $f \approx 0.3$ is derived for Mn^{2+}-doped cubic fluoroperovskites. This figure can be compared with $f \leqslant 0.1$ obtained for Cr^{3+} in elpasolites [48] or Fe^{3+} in fluoroperovskites [49] where the elastic coupling of the transition metal complex with the rest of the lattice is certainly smaller.

4.2. Consistency of the KSCED embedding formalism

The results gathered in table 1 have been derived keeping $\rho_{II}(\mathbf{r})$ frozen while finding the right density of region I, $\rho_I(\mathbf{r})$, where active electrons are located. For exploring the consistency of the method one can calculate in a second step the right density of region II keeping $\rho_I(\mathbf{r})$ frozen. Let us designate such a density by $\rho'_{II}(\mathbf{r})$. In a subsequent freeze and thaw step the correct density of region I is again calculated but using now the relaxed density $\rho'_{II}(\mathbf{r})$ as the frozen density of region II. Let us call this new density of region I $\rho'_I(\mathbf{r})$. The consistency of the method requires that $\rho'_I(\mathbf{r})$ is very close to $\rho_I(\mathbf{r})$. In table 2 the equilibrium Mn^{2+}–F^- distances

Table 2. Mn^{2+}–F^- equilibrium distances obtained in the KSCED calculations (13 + 8 clusters) using $\rho_{II}(\mathbf{r})$ (unrelaxed density) and $\rho'_{II}(\mathbf{r})$ (relaxed density). Units are in Å.

Lattice	$\rho_{II}(\mathbf{r})$	$\rho'_{II}(\mathbf{r})$
$KMgF_3$	2.064	2.061
$KZnF_3$	2.107	2.108
$RbCdF_3$	2.166	2.164
$RbCaF_3$	2.130	2.129

Table 3. Values of the $10Dq$ splitting parameter obtained from orbital energy differences in the ground state through KSCED calculations (13+8 and 21+36 schemes). Experimental values, taken from [7, 10], are shown for comparison. Energies are in eV. Values of the $10Dq$ decay exponent n are also given.

	(13 + 8)		(21 + 36)		Experimental
	$10Dq$	n	$10Dq$	n	$10Dq$
$KMgF_3$	1.182	4.50	1.176	4.72	1.045
$KZnF_3$	1.047	4.16	1.066	4.67	1.018
$RbCdF_3$	0.974	4.33	0.972	4.58	0.900
$RbCaF_3$	1.091	3.93	1.070	4.98	0.905

calculated with $\rho'_I(\mathbf{r})$ are compared to those derived from $\rho_I(\mathbf{r})$. As the two R_0 values differ by less than 0.15%, this fact thus supports the consistency of the KSCED embedding formalism.

4.3. $10Dq$ *and* $\mathrm{d}10Dq/\mathrm{d}R$ *values for* MnF_6^{4-} *in cubic fluoroperovskites*

$10Dq$ values calculated at the equilibrium distance, R_0, for the studied AMF_3:Mn^{2+} systems are displayed in table 3 and compared to experimental values [6, 7, 12]. In this case the results have been derived using both 13 + 8 and 21 + 36 partition schemes. Similar results are obtained in both cases. In table 3 the value of the exponent n defined in equation (14), characterizing the variation of $10Dq$ of a given system under hydrostatic pressure, is reported as well. For achieving this goal calculations have been carried out for different values of the lattice parameter a, finding for each one the equilibrium Mn^{2+}–F^- distance and the corresponding $10Dq$ value. Very similar values of the exponent n (lying between 4 and 5) are found for different AMF_3:Mn^{2+} systems.

Let us now focus on $10Dq$ values of different AMF_3:Mn^{2+} systems at zero pressure when the equilibrium Mn^2–F^- distance is R_0. Looking at the data collected in table 3 it turns out that the chemical exponent n^c is essentially coincident with the hydrostatic exponent n in agreement with a previous guess [7]. Experimentally a value $n^c = 4.7$ has been reported [10, 7]. This result thus supports the conclusion that in the present systems $10Dq$ is basically originated in the MnF_6^{4-} complex and only depends on the actual Mn^{2+}–F^- distance. In other words, the $10Dq$ variations produced by hydrostatic or chemical pressures but leading to the same change of Mn^{2+}–F^- distance would essentially be the same. This statement is supported by the results gathered in table 4, where the $10Dq$ values calculated for $KMgF_3$:Mn^{2+} and $RbCdF_3$:Mn^{2+} *at the same distance* are reported. In table 4 are also shown the values of the corresponding lattice parameters where this situation is produced. It can be seen that the computed $10Dq$ value for $KMgF_3$:Mn^{2+} at $R = 2.11$ Å coincides with that for $RbCdF_3$:Mn^{2+} at the same distance.

From a microscopic standpoint it has been shown that $\mathrm{d}10Dq/\mathrm{d}R$ for the MnF_6^{4-} complex depends to a great extent on the *small 2s–2p hybridization* on ligands [50, 3]. A similar situation

Table 4. Comparison between Mn^{2+}–F^- equilibrium distances, R_0, and $10Dq$ splittings obtained from KSCED (13 + 8 clusters) and KS calculations. Distances are in Å and energies in eV.

		R_0		$10Dq$	
Lattice	R_H	KSCED	KS	KSCED	KS
$KMgF_3$	2.027	2.11	2.104	8626	9445
$RbCdF_3$	2.160	2.11	2.11	8430	9175

Table 5. Mn^{2+}–F^- equilibrium distances, R_0, and vibration frequencies of a_{1g} and e_g modes obtained through KSCED (13 + 8 cluster) and KS calculations, considering different lattice parameters for each compound. Frequencies are in cm^{-1} and distances in Å.

		KSCED 13 + 8			KS		
Lattice	R_H	R_0	$\hbar\omega_a$	$\hbar\omega_e$	R_0	$\hbar\omega_a$	$\hbar\omega_e$
$KMgF_3$	1.945	2.019	607	515	2.019	616	531
$KMgF_3$	1.9865	2.064	564	466	2.068	554	471
$KMgF_3$	2.027	2.093	525	424	2.103	511	420
$KZnF_3$	1.986	2.057	557	458	2.057	545	477
$KZnF_3$	2.027	2.107	498	403	2.103	504	425
$KZnF_3$	2.068	2.145	452	352	2.149	456	370
$RbCdF_3$	2.160	2.109	477	377	2.117	462	377
$RbCdF_3$	2.200	2.166	412	318	2.158	421	330
$RbCdF_3$	2.240	2.191	377	270	2.198	385	283

has been found for other systems like CrF_6^{3-} or CrO_4^{4-} [51, 52]. Experimental values of the exponent n close to 5 are still justified through the crystal field model [28] despite it predicting $10Dq$ values which are one order of magnitude smaller than the right ones [3].

4.4. Local vibrations and Grüneisen parameters

Calculated values of ω_e and ω_a frequencies by means of the KSCED embedding formalism (13+8 partition scheme) for several AMF_3:Mn^{2+} systems are reported in table 5 and compared to those derived through the conventional KS method. As a salient feature, aside from the frequencies corresponding to the lattice parameter at zero pressure, results are also collected for other a values which are experimentally attainable under hydrostatic pressure. This allows one to compare very easily the action of hydrostatic and chemical pressures upon local frequencies. It is worth noting that γ_e was not calculated in a previous work [13].

Let us first consider the R-dependence of $\hbar\omega_a$ values found for $KMgF_3$:Mn^{2+}. It can be seen in table 5 that on passing from $R = 2.064$ to 2.093 Å, $\hbar\omega_a$ decreases by 39 cm^{-1}, thus implying a reduction of 13.5 cm^{-1}/pm. However, a bigger reduction of 19.5 cm^{-1}/pm is found when comparing $\hbar\omega_a = 525$ cm^{-1} for $KMgF_3$:Mn^{2+} at $R = 2.093$ Å with $\hbar\omega_a = 477$ cm^{-1} for $RbCdF_3$:Mn^{2+} at $R = 2.109$ Å. Along this line it is also important to notice that the $\hbar\omega_a$ and $\hbar\omega_e$ values for $KZnF_3$:Mn^{2+} and $RbCdF_3$:Mn^{2+} calculated at the same distance (2.108 Å) *are not* the same. In agreement with previous findings [13] all these facts thus support the conclusion that: (i) the values of local frequencies ω_e and ω_a are not only a function of the impurity–ligand distance, R; (ii) if the variation of the Mn^{2+}–F^- distance is the same the changes of ω_e and ω_a induced by a chemical pressure are bigger than those produced on a single system by the hydrostatic pressure. These conclusions are also reflected in the different values of Grüneisen constants γ_i ($i = a, e$) (extracted in table 6 from the results of table 5) and the chemical γ_i^c parameters. For instance, γ_a (γ_e) for KMF_3:Mn^{2+} (M = Mg, Zn) is

Table 6. Grüneisen constants for a_{1g} and e_g modes obtained from KSCED (13 + 8 clusters) and KS calculations.

	γ_a		γ_e	
Lattice	KSCED	KS	KSCED	KS
$KMgF_3$	1.3	1.5	1.8	1.9
$KZnF_3$	1.7	1.4	2.1	1.9
$RbCdF_3$	2.0	1.6	2.9	2.5

found to be less than 1.7 (2.1) while $\gamma_a^c = 2.2$ and $\gamma_e^c = 2.8$. It can be seen that the results derived through the KSCED and KS methods are certainly very close. The present results thus support the conclusion that γ_e^c values close to 3 are certainly possible. Although the same conclusion was obtained in a previous work [13] using older KS-DFT calculations, there are, however, some relevant differences with the results obtained in the present work. So, the value $\gamma_a^c = 2.2$ obtained in the present work is somewhat smaller than $\gamma_a^c = 3.2$ reached in [13]. Moreover, in [13] the values of $\hbar\omega_a$ for $KMgF_3$:Mn^{2+}, $KZnF_3$:Mn^{2+} and $RbCdF_3$:Mn^{2+} were found to be equal to 556, 454 and 353 cm^{-1}, respectively. Therefore, although the value $\hbar\omega_a = 556\ cm^{-1}$ for $KMgF_3$:Mn^{2+} at zero pressure is quite close to those gathered in table 5, the figure $\hbar\omega_a = 454\ cm^{-1}$ derived for $KZnF_3$:Mn^{2+} is, however, about 50 cm^{-1} smaller than those reached in the present work (table 5).

As previously noticed [13], the difference between γ_i and γ_i^c parameters emphasizes the elastic coupling of the MnF_6^{4-} complex with close ions of the rest of the AMF_3 lattice. Along a $\langle 100 \rangle$ direction a F^- ligand is placed between a Mn^{2+} impurity and a M^{2+} ion of the host lattice. Let us designate by k and k' the force constants associated with Mn–F and F–M bonds, respectively. In a simple model a quantity like $\hbar\omega_a^2$ depends on $k + k'$. When there is a significant elastic coupling of the complex with the rest of the lattice k' cannot be neglected, and thus $\hbar\omega_a$ and $\hbar\omega_e$ can be modified just by changing the nature of the host cation M^{2+} even if R is kept.

The low-temperature luminescence spectrum of $KMgF_3$:Mn^{2+} [8] shows a weak vibrational progression involving an energy step $\hbar\omega_v = 570\ cm^{-1}$. Bearing in mind the calculated $\hbar\omega_a$ values for $KMgF_3$:Mn^{2+} at zero pressure (table 5) through the KSCED and KS methods (564 and 554 cm^{-1}, respectively), such a vibrational progression can reasonably be associated with the a_{1g} mode of MnF_6^{4-} embedded in $KMgF_3$. This result thus supports a previous conclusion [13]. Therefore, the $\hbar\omega_a$ value for MnF_6^{4-} in $KMgF_3$ is a little higher than the value $\hbar\omega_a = 538\ cm^{-1}$ measured by Raman spectroscopy for the $(NH_4)_3FeF_6$ compound involving the trivalent Fe^{3+} ion [31]. This surprising result [32] can be understood by taking into account the big effects of chemical pressure along the series of Mn^{2+}-doped fluoroperovskites. In fact, for $R_0 = 2.13$ Å (corresponding to the sum of ionic radii of Mn^{2+} and F^-) $\hbar\omega_a$ values smaller than 490 cm^{-1} are expected for MnF_6^{4-} in fluoroperovskites.

The present results for $KZnF_3$:Mn^{2+} (table 5) give $\hbar\omega_a = 500\ cm^{-1}$, which is a bit smaller than $\hbar\omega_v = 540\ cm^{-1}$ measured in the corresponding luminescence spectrum. However, it can be noticed that in the present calculations the obtained R_0 values are 1–2 pm higher than the figure derived from the analysis of experimental optical and electron paramagnetic resonance (EPR) parameters [6, 7, 10, 12]. Bearing in mind the results of table 6, a reduction of ∼2 pm in the R_0 value would imply an increase of $\hbar\omega_a$ close to 30 cm^{-1}.

4.5. Coupling constants for the $^4T_{1g}$ state: Stokes shift of AMF_3:Mn^{2+} at zero pressure

In a first step, values of the V_a and V_e coupling constants have been derived from the variations of energies of orbitals of the ground state of the MnF_6^{4-} complex under isotropic or Q_θ

Table 7. Linear coupling constants, V_i, Huang–Rhys factors, S_i, and Stokes shift (E) for A_{1g} and E_g modes obtained from orbital splittings in KSCED (13 + 8) calculations. Values of V are in cm^{-1}/pm and E in cm^{-1}. Experimental E_S values [10] are also given.

Lattice	R_0	V_a	S_A	$2E_a$	V_e	S_e	$2E_e$	E_S^0	E_S (experimental)
$KMgF_3$	2.064	88.0	0.38	428	66.3	0.38	354	782	1205
$KZnF_3$	2.107	71.4	0.36	363	54	0.39	316	679	1430
$RbCdF_3$	2.166	65.3	0.53	442	49	0.67	424	866	1560

distortions, respectively [26, 23]. For instance, under a $Q_\theta \sim 3z^2 - r^2$ distortion of the octahedron there is a splitting, Δ_e, between the x^2–y^2 and $3z^2$–r^2 levels of the e_g orbital as well as a splitting, Δ_t, between the xy and the (xz, yz) levels of the t_{2g} shell. For an elongated octahedron Q_θ, Δ_e and Δ_t are all positive. A reasonable expression for V_e corresponding to the first excited state $^4T_{1g}$ of the MnF_6^{4-} complex is given by [26]

$$V_e(^4T_{1g}) = (1/2)\{\partial(\Delta_e - 4\Delta_t/3)/\partial Q_\theta\}. \tag{18}$$

Values of V_a and V_e coupling constants calculated by this procedure at the equilibrium distance at zero pressure for several Mn^{2+}-doped fluoroperovskites are reported in table 7. In this table the calculated values of Huang–Rhys factors, S_a and S_e, and the quantities $E_S(i)$ ($i = a, e$) are also collected. The calculated E_S^0 value is compared to experimental results of E_S at room temperature.

The results for V_a and V_e constants gathered in table 7 are quite similar to those previously derived by means of both MS-Xα and Extended Hückel methods [23, 26, 13]. They lead to S_a values smaller than unity and thus support the existence of weak progressions involving the a_{1g} mode for both $KMgF_3$:Mn^{2+} and $KZnF_3$:Mn^{2+} systems [8]. They give rise to an increase of S_a, S_e and also E_S^0 as long as the equilibrium distance, R_0, increases. By contrast, similarly to what is obtained for $10Dq$, V_a and V_e are found to decrease when R_0 increases. From table 7 it is derived that $n_a^c \approx n_e^c \approx 5.5$.

As shown in table 7, the experimental Stokes shift, E_S, has been found to increase on going from $KMgF_3$:Mn^{2+} to $RbCdF_3$:Mn^{2+} [10]. The difference between the experimental Stokes shift and the calculated E_S^0 quantity can reasonably be ascribed to the odd mode assistance depicted by equation (9). To reproduce the E_S^0 quantity (quite sensitive to values of V_i constants and ω_i frequencies) along a series of *different* host lattices is not a simple task. The calculated decrease of E_S^0 (table 7) on passing from $KMgF_3$:Mn^{2+} to $KZnF_3$:Mn^{2+} can be ascribed to an underestimation of V_a.

When E_i ($i = a, e$) and E_S^0 are derived looking *directly* at the relaxed $^4T_{1g}$ excited state (table 8) a similar picture to that of table 7 is obtained. For the sake of completeness the equilibrium values of the Mn^2–F^- distance, $R_0(^4T_{1g})$, and Q_θ coordinate, Q_θ^0, are also reported in table 8. It can be noticed that $R_0(^4T_{1g})$ is about 1% smaller than R_0 for the ground state $^6A_{1g}$. This result is qualitatively consistent with the different electronic configuration exhibited by the ground ($t_{2g}^3e_g^2$) and the $^4T_{1g}$($t_{2g}^4e_g^1$) states. Therefore, on passing from $^6A_{1g}$ to $^4T_{1g}$ there is a transfer of an antibonding e_g electron with σ-character to another antibonding level but with π-character. An elongated octahedron is well described by the axial, R_{ax}, and equatorial, R_{eq}, distances given by

$$R_{ax} = R_0 + 2\eta; \qquad R_{eq} = R_0 - \eta \qquad (\eta > 0). \tag{19}$$

The relation of the η parameter describing the tetragonality with the Q_θ coordinate is simply given by [21, 53]

$$Q_\theta = \sqrt{12}\eta. \tag{20}$$

Table 8. Stokes shifts contributions, $2E_i$, from $i = a_{1g}$, e_g modes derived directly from equilibrium geometries of $^6A_1$ and $^4T_1$ states obtained with the KS method. Mn^{2+}–F^- equilibrium distances, R_0, for both states are also shown. Distances are in Å and energies in cm^{-1}. Experimental E_S values from [10] are also given.

Lattice	R_0 ($^6A_1$)	R_0 ($^4T_1$)	Q^0_θ (Å)	$2E_a$	$2E_e$	E^0_S	E_S (experimental)
$KMgF_3$	2.064	2.046	0.044	480	454	934	1205
$KZnF_3$	2.107	2.078	0.040	462	316	777	1430
$RbCdF_3$	2.166	2.126	0.063	581	462	1043	1560

Therefore, the Jahn–Teller distortion in the relaxed $^4T_{1g}$ state leads to an axial distance, R_{ax}, which is only 1.7% higher than $R_0(^4T_{1g})$ for $RbCdF_3$:Mn^{2+}. This figure, together with the value $E_e = 290\ cm^{-1}$ for the Jahn–Teller energy, emphasizes that the Jahn–Teller effect in the $^4T_{1g}$ state of MnF_6^{4-} is weaker than in the ground state of NaCl:Rh^{2+} [53].

Bearing in mind equations (8), (9), (15), (16) the R-dependence of E_i and S_i quantities is just given by

$$S_i \propto R_e^{9\gamma_i^c - 2n_i^c}; \qquad E_i \propto R_e^{6\gamma_i^c - 2n_i^c} \quad (i = a, e). \tag{21}$$

Therefore, if $n_a^c \approx n_e^c \approx 6$ (table 7) the high values of the chemical Grüneisen parameters $\gamma_a^c = 2.2$ and specially $\gamma_e^c = 2.8$ are consistent with the increase of the experimental Stokes shift when R_0 increases as a result of a different chemical pressure [10].

For the sake of completeness an estimation of the V_t coupling constant has also been carried out. In a good approximation a $^4T_{1g}$ state in O_h is simply described by the Slater determinant

$$|^4T_{1g}\rangle = |yz\uparrow, xz\uparrow, xy\uparrow, xy\downarrow, 3z^2 - r^2\uparrow|. \tag{22}$$

Let us consider the effects of a trigonal distortion on the $^4T_{1g}$ state one-electron orbitals involved in (22). According to equation (8), a trigonal distortion described by $Q_{xy} = Q_{xz} = Q_{yz} = Q$ splits the $^4T_{1g}$ state into a doublet and a singlet separated by $3V_tQ$. As the degeneracy in the e_g orbital remains under this D_{3h} distortion the splitting $3V_tQ$ is related to the splitting, Δ_t, between the levels of the t_{2g} shell. Writing $\Delta_t = \beta Q$ it is found that $V_t = \beta/3$. Through this procedure there has been derived for $KMgF_3$:Mn^{2+} at $R_0 = 2.06$ Å a value $V_t = 8\ cm^{-1}/pm$. The calculated value for $\hbar\omega_t$ corresponding to the t_{2g} shear mode has been found to be equal to 219 cm^{-1} and thus $E_t = 22\ cm^{-1}$ according to equation (8). Therefore, the estimated V_t and E_t values are both one order of magnitude smaller than the V_i and E_i ($i = a, e$) quantities displayed in tables 7 and 8. Due to this fact, it can reasonably be explained that E^0_S can be understood through the coupling with the two a_{1g} and e_g stretching modes. For octahedral CrX_6^{3-} units (X = F, Cl and Br) in cubic elpasolites no experimental evidence of any coupling of the first excited state, $^4T_{2g}$, with the t_{2g} shear mode has been reported [24, 28, 44, 45].

4.6. Stokes shift of $KMgF_3$:Mn^{2+} under hydrostatic pressure

The influence of a hydrostatic pressure on V_a and V_e constants and the E^0_S quantity has also been simulated. In table 9 results on these variables for $KMgF_3$:Mn^{2+} are reported from calculations carried out at three different values of the lattice parameter a. As expected, both V_a and V_e constants decrease when the lattice parameter a and the equilibrium Mn^{2+}–F^- distance, R_0, (at different pressures) increase. The corresponding exponents n_a and n_e are collected in table 10. It can be seen that they are not far from the values of the chemical exponents n_a^c and n_e^c discussed in the previous section. Nevertheless, a different behaviour appears when

Table 9. Linear coupling constants, V_i (in cm^{-1}/pm), Huang–Rhys factors, S_i, and Stokes shifts, $2E_i$ (in cm^{-1}) ($i = a_{1g}, e_g$) obtained from orbital splittings in KSCED (13 + 8) calculations for $KMgF_3$ with different lattice constants.

R_H	R_0	V_a	S_a	$2E_a$	V_e	S_e	$2E_e$	E_S^0
1.945	2.019	99.8	0.39	477	74.1	0.35	363	840
1.987	2.064	88.0	0.38	430	66.3	0.38	354	784
2.027	2.093	78.4	0.37	394	62.4	0.45	379	773

Table 10. Decay exponent with the distance, n_i, of linear coupling constants V_i ($i = a_{1g}, e_g$) obtained from KSCED (13 + 8 clusters) and KS calculations.

	n_a		n_e	
Lattice	KSCED	KS	KSCED	KS
$KMgF_3$	6.7	5.7	4.8	5.1
$KZnF_3$	5.6	5.8	4.9	4.8
$RbCdF_3$	6.5	6.3	4.8	5.2

looking at the E_S^0 quantity which is not found to increase when R does. By contrast, when R increases by 3.7%, E_S^0 is found to *decrease* by 8%. This significant difference with the behaviour of E_S^0 under chemical pressure can easily be rationalized by taking into account the values of Grüneisen constants (table 6) and n_a and n_e exponents given in table 10. Similarly to the discussion given in the preceding section there can be written

$$E_i \propto R^{6\gamma_i - 2n_i} \quad (i = a, e). \tag{23}$$

Therefore, if $n_a = 6$ and $\gamma_a = 1.4$ then $6\gamma_a - 2n_a = -3.6$ and thus E_a increases when R is reduced by an applied hydrostatic pressure.

In a first study on Huang–Rhys factors it was suggested that they would tend to decrease when the metal–ligand distance is reduced. This trend is well followed by the results collected in tables 10 and 7. Experimental results carried out on $Cs_2NaScCl_6:Cr^{3+}$ have verified [28] that, in this case, S_a and S_e decrease when a hydrostatic pressure is applied.

4.7. Elastic coupling of the MnF_6^{4-} complex to the host lattice

A simple way to visualize the influence of the elastic coupling of the MnF_6^{4-} complex with close ions of the rest of the lattice is given in this section. When a MnF_6^{4-} complex is inserted in a fluoroperovskite its equilibrium distance at zero pressure is R_0. However, if *only* the *isolated* MnF_6^{4-} complex is considered it is necessary to apply an external force on each ligand in order the keep the impurity–ligand distance equal to R_0. Therefore, the ground state energy of the isolated complex around $Q_a = 0$ can now be written as

$$E(Q_a) = E_0 + f\,Q_a + (1/2)k\,Q_a^2 + \cdots. \tag{24}$$

If the linear term is balanced by an external force it turns out that the corresponding frequency for the isolated complex, termed ω_{ai}, is just given by

$$\omega_{ai}^2 = k/M_L. \tag{25}$$

If the motion of ligands for the complex *in the lattice* is also influenced by their interaction with close Mg^{2+} cations it can be expected that $\omega_{ai}^2 < \omega_a^2$. Simple KS calculations carried out on $KMgF_3:Mn^{2+}$ give $\hbar\omega_{ai} = 284\ cm^{-1}$ for $R_0 = 2.068$ Å, a figure which is certainly

smaller than $\hbar\omega_a = 554\ cm^{-1}$ reported in table 5. For estimating the contribution of the force constant k' to the value of $\hbar\omega_a$ an *isolated* MgF_6^{4-} octahedron has also been taken into account. Following a similar process to that described for MnF_6^{4-} the corresponding frequency ω_{Mi} can equally be determined. This frequency reflects the k' force constant through the expression

$$\omega_{Mi}^2 = k'/M_L. \tag{26}$$

For $KMgF_3$ it has been found $\hbar\omega_{Mi} = 450\ cm^{-1}$. Moreover, assuming as a reasonable first approximation that

$$\omega_a^2 = (k + k')/M_L = \omega_{ai}^2 + \omega_{Mi}^2, \tag{27}$$

a value $\hbar\omega_a = 532\ cm^{-1}$ is derived, not far from $\hbar\omega_a = 554\ cm^{-1}$ collected in table 5. A similar picture is obtained for other lattices. For instance, for $RbCdF_3$:Mn^{2+} the values $\hbar\omega_{ai} = 272\ cm^{-1}$ and $\hbar\omega_{Mi} = 358\ cm^{-1}$ have been obtained in the present calculations. These results prove in an easy way that although the M^{2+} cation can be considered at rest the motion of ligands in a_{1g} and e_g modes is greatly influenced by the F^-–M^{2+} force constant.

A similar analysis performed for Cr^{3+} in elpasolites [48] showed that in this case $k > k'$. This fact indicates that in elpasolite lattices the elastic coupling of the complex to the rest of the lattice tends to be smaller than in the case of perovskites, a conclusion which is reasonable when looking at the two crystal structures. However, it is worth noting that in a perovskite lattice the decoupling form the rest of the lattice can be increased if impurities with a nominal charge higher than 2 (like Fe^{3+} or Cr^{3+}) are introduced [49].

5. Final remarks

A detailed study of model systems corresponding to Mn^{2+} impurities in cubic AMF_3 fluoroperovskites has been carried out by means of two methods based in the DFT. The main trends are reproduced by both methods. Results obtained by means of the KSCED orbital-free embedding formalism show that a good description is reached placing only 13 atoms in region I and 8 in the frozen region II.

It has been demonstrated that while an electronic parameter like $10Dq$ essentially depends on the Mn^{2+}–F^- distance this is no longer true as far as local vibration frequencies are concerned. Such frequencies have been shown to be dominated by the interaction between F^- ligands and nearest M^{2+} ions lying along bonding directions. This fact is responsible for the high ω_a values observed [8] for $KMgF_3$:Mn^{2+} and $KZnF_3$:Mn^{2+}. Moreover, it also explains the huge variations of ω_e and ω_a frequencies when the host lattice is changed, as well as the increase of Huang–Rhys factors and the Stokes shift following the host lattice parameter. It is worthwhile remarking that this increase of the Stokes shift, E_S, on passing from $KMgF_3$:Mn^{2+} to $RbCdF_3$:Mn^{2+} is compensated by the increase of the energy difference, E_G, between $^4T_{1g}$ and the ground state, making $2\Lambda = E_S/E_G$ to be nearly constant along the series of cubic fluoroperovskites [10, 13, 40]. As was already pointed out, an increase of the Λ parameter favours the luminescence quenching [18, 13].

The importance of the elastic coupling of the complex to the rest of the lattice in connection with the existence of coherent tunnelling in $E \otimes e$ Jahn–Teller systems has recently been emphasized [54]. It has been shown that the barrier among equivalent configurations is dominated by the anharmonicity of the e_g mode [53] which in turn can be softened by an increase of the elastic coupling of the complex to the rest of the lattice [54].

Due to the *localized character* of the interaction between active electrons and local vibrations, the normal coordinates describing the distortion related to the $^6A_{1g} \rightarrow ^4T_{1g}$ excitation essentially involve coordinates of ligand ions. According to the theory of elasticity in

three dimensions, it is expected that if the Mn^{2+}–F^- distance changes by 2% then the Mn^{2+}–Mg^{2+} distance with second neighbours along ⟨100⟩ directions would change by ∼0.5%. The vibration of ligand ions against the wall formed by the host lattice should be viewed as a resonant mode, as suggested earlier by Sturge [22]. For instance, the highest frequency of the $KMgF_3$ lattice is close to 600 cm^{-1} [55]. It is important to notice that after a Franck–Condon excitation the creation of *local* vibration quanta has been observed. This energy is later transferred to the host lattice phonons [29].

The present results support the conclusion that E_S^0 is determined by the coupling with a_{1g} and e_g local modes while the coupling with the t_{2g} shear mode is not relevant. However, this situation can be different when the local geometry changes from octahedral to cubic or tetrahedral. Work along this line is now under way.

Acknowledgments

Partial support by the Spanish Ministerio de Ciencia y Tecnología under the Project 'Origin of instabilities in doped and ferroelectric materials' is acknowledged. TAW is grateful for the support by the Swiss National Scientific Foundation.

References

[1] Sugano S and Shulman R G 1963 *Phys. Rev.* B **130** 517
[2] Jorgensen C K 1971 *Modern Aspects of Ligand Field Theory* (Amsterdam: North-Holland)
[3] Moreno M, Aramburu J A and Barriuso M T 2004 *Struct. Bonding* **106** 127
[4] Ferguson J, Güdel H U, Krausz E R and Guggenheim H J 1974 *Mol. Phys.* **28** 879
[5] Rousseau J J, Leble A and Fayet J C 1978 *J. Physique* **39** 1215
[6] Barriuso M T and Moreno M 1984 *Phys. Rev.* B **29** 3623
[7] Rodríguez F and Moreno M 1986 *J. Chem. Phys.* **84** 692
[8] Rodríguez F, Riesen H and Güdel H U 1991 *J. Lumin.* **50** 101
[9] Spaeth J-M, Niklas J R and Bartram R H 1992 *Structural Analysis of Point Defects in Solids* (Berlin: Springer)
[10] Marco de Lucas M, Rodríguez F and Moreno M 1994 *Phys. Rev.* B **50** 2760
[11] Lahoz F, Alcalá R, Pawlik Th and Spaeth J-M 1996 *J. Phys.: Condens. Matter* **8** 7355
[12] Barriuso M T, Aramburu J A and Moreno M 1999 *J. Phys.: Condens. Matter* **11** L525
[13] Barriuso M T, Moreno M and Aramburu J A 2002 *Phys. Rev.* B **65** 064441
[14] van der Kolk E, Dorenbos P, van Eijk C W E, Vink A P, Weil M and Chaminade J P 2004 *J. Appl. Phys.* **95** 7867
[15] Wesolowski T A 1997 *J. Chem. Phys.* **106** 8516
[16] Zbiri M, Atanasov M, Daul C, García-Lastra J M and Wesolowski T A 2004 *Chem. Phys. Lett.* **397** 441
[17] Wesolowski T A 2005 *Computational Chemistry: Reviews of Current Trends* vol 11, ed J Leszczynski (Singapore: World Scientific) at press
[18] Bartram R H and Stoneham M 1975 *Solid State Commun.* **17** 1593
[19] Blasse G and Grabmaier B C 1994 *Luminescent Materials* (Berlin: Springer)
[20] Dorenbos P 2000 *J. Lumin.* **91** 106
[21] Bersuker I and Polinger V Z 1984 *The Dynamical Jahn–Teller Effect in Localized Systems* ed Yu Perlin and W Wagner (Amsterdam: North-Holland)
[22] Sturge M D 1971 *Solid State Commun.* **9** 899
[23] Moreno M, Aramburu J A and Barriuso M T 1992 *J. Phys.: Condens. Matter* **4** 9481
[24] Dolan J F, Rinzler A G, Kappers L A and Bartram R H 1992 *J. Phys. Chem. Solids* **53** 905
[25] Villacampa B, Casas González J, Alcalá R and Alonso P J 1991 *J. Phys.: Condens. Matter* **3** 8281
[26] Barriuso M T, Aramburu J A and Moreno M 1996 *Phys. Status Solidi* b **193** 193
[27] Gilardoni F, Weber J, Bellafrouh K, Daul C and Güdel H U 1996 *J. Chem. Phys.* **104** 7624
[28] Wenger O S, Valiente R and Güdel H U 2001 *J. Chem. Phys.* **115** 3819
[29] Calistru D M, Demos S G and Alfano R R 1997 *Phys. Rev. Lett.* **78** 374
[30] Goldberg V, Moncorge R, Pacheco D and Di Bartolo B 1988 *Luminescence of Inorganic Solids* (New York: Plenum)
[31] Wieghardt K and Eysel H H 1970 *Z. Naturf.* b **25** 105
[32] Nakamoto K 1986 *Infrared and Raman Spectra of Inorganic and Coordination Compounds* 4th edn (New York: Wiley)

[33] Wesolowski T A and Warshel A 1993 *J. Phys. Chem.* **97** 8050
[34] Kohn W and Sham L J 1965 *Phys. Rev.* A **140** 1133
[35] Casida M E, Daul C, Goursot A, Koester A, Pettersson L G M, Proynov E, St-Amant A, Salahub D R, Chretien S, Duarte H, Godbout N, Guan J, Jamorski C, Leboeuf M, Malkin V, Malkina O, Nyberg M, Pedocchi L, Sim F and Vela A 1998 deMon code release 3.5
St-Amant A and Salahub D R 1990 *Chem. Phys. Lett.* **169** 387
St-Amant A 1992 *PhD Thesis* University of Montreal
Wesolowski T A and Weber J 1996 Implementation of the KSCED formalism *Chem. Phys. Lett.* **248** 71
[36] Becke A D 1988 *Phys. Rev.* A **38** 3098
[37] Perdew J P 1986 *Phys. Rev.* B **33** 8822
[38] Lembarski A and Chermette H 1994 *Phys. Rev.* A **50** 5328
[39] te Velde G, Bickelhaupt F M, Baerends E J, Fonseca Guerra C, van Gisbergen S J A, Snijders J G and Ziegler T 2001 *J. Comput. Chem.* **22** 931
[40] Marco de Lucas M C, Moreno M, Rodríguez F and Baranov P G 1996 *J. Phys.: Condens. Matter* **8** 2457
[41] Pedrini Ch, Mc Clure D S and Anderson C H 1979 *J. Chem. Phys.* **70** 4959
[42] Dorenbos P 2003 *J. Phys.: Condens. Matter* **15** 2645
[43] Solomon E I and McClure D S 1974 *Phys. Rev.* B **9** 4690
[44] Knochenmuss R, Reber C, Rajasekharan M V and Gudel H U 1986 *J. Chem. Phys.* **85** 4280
[45] Marco de Lucas M C, Rodríguez F, Dance J M, Moreno M and Tressaud A 1991 *J. Lumin.* **48/49** 553
[46] Galli B, Hauser A and Güdel H U 1985 *Inorg. Chem.* **24** 2271
[47] Toyozawa Y and Inoue M 1966 *J. Phys. Soc. Japan* **21** 1663
[48] Aramburu J A, Moreno M, Doclo K, Daul C and Barriuso M T 1999 *J. Chem. Phys.* **110** 1497
[49] Aramburu J A, Paredes J I, Barriuso M T and Moreno M 2000 *Phys. Rev.* B **61** 6525
[50] Moreno M, Barriuso M T and Aramburu J A 1994 *Int. J. Quantum Chem.* **52** 829
[51] Moreno M, Aramburu J A and Barriuso M T 1997 *Phys. Rev.* B **56** 14423
[52] Wissing K, Barriuso M T, Aramburu J A and Moreno M 1999 *J. Chem. Phys.* **111** 10217
[53] García-Fernandez P, Bersuker I, Aramburu J A, Barriuso M T and Moreno M 2005 *Phys. Rev.* B **71** 184117
[54] García-Fernandez P, Sousa C, Aramburu J A, Barriuso M T and Moreno M 2005 *Phys. Rev.* B **72** 155107
[55] Salaun S, Mortier M, Geloand J Y, Rousseau M and Hennion B 1993 *J. Phys.: Condens. Matter* **5** 7615